Response Properties of Furan Homologues by Time-Dependent Density Functional Theory

Wolfgang Hieringer, Stan J. A. van Gisbergen, and Evert Jan Baerends*

Theoretische Chemie, Faculteit Exacte Wetenschappen, Vrije Universiteit Amsterdam, De Boelelaan 1083, 1081 HV Amsterdam, The Netherlands

Received: March 29, 2002; In Final Form: August 20, 2002

The electronic excitations and frequency-dependent electronic second hyperpolarizability $\gamma(-\omega;\omega,\omega,-\omega)$ of the five-ring heterocycles furan, thiophene, selenophene, and tellurophene have been reinvestigated using time-dependent density functional theory. Aspects of basis set saturation, the performance of exchange-correlation potentials, and relativistic effects are discussed. Increased hyperpolarizabilities for molecular dimer species suggest that intermolecular interactions may provide a simple explanation for the large deviations between recent ab initio calculations and experimental condensed-phase data.

1. Introduction

The response properties of the five-ring heterocycles furan, thiophene, selenophene, and tellurophene C_4H_4X (X = O, S, Se, Te) have recently attracted much interest due to their advantageous application as molecular bridges in donor−acceptor compounds having nonlinear optical properties.[1,2] The chemical and physical properties of these molecules and their derivatives were shown to be strongly dependent on the nature of the heteroatom. For example, following a number of theoretical and experimental indicators, the aromaticities of the conjugated rings change in the order thiophene > selenophene > tellurophene > furan.[3] The electronic structure of the compounds has been investigated in considerable detail using a variety of spectroscopic techniques.

Recently, Kamada et al. have provided accurate data on the electronic second hyperpolarizability of the title compounds in the liquid state using a femtosecond optically heterodyne-detected optical Kerr effect (OHD-OKE) experiment.[4,5] A steep increase of the nonlinear optical response with the atomic number of the heteroatom was observed, triggering extensive ab initio calculations on various static response properties of these molecules.[6−9] Although a modest influence of the heteroatom on the second hyperpolarizability was predicted by these theoretical calculations, the large increase observed experimentally could not be satisfactorily reproduced. Technical limitations of the current theoretical calculations, such as lack of frequency dependence, basis set insufficiencies, and neglect of relativistic effects, have been discussed as possible explanations for the problem.[6,7] The origin of the discrepancy between theory and experiment remained unexplained so far, however.

In this study, we present the first calculations of the frequency-dependent (optical Kerr effect, OKE) second hyperpolarizabilities of furan, thiophene, selenophene, and tellurophene using time-dependent density functional theory (TDDFT) in combination with a variety of exchange-correlation functionals and basis sets and relate the results to the electronic structure and the excitation spectrum of the compounds. We also address the influence of relativity and the effect of intermolecular interactions as present in the condensed phase. On the basis of our data, we discuss several possibilities to explain the large discrepancies between calculated and experimental values that have been observed in earlier studies on tellurophene. Moreover, the results will provide information about the reliability of current TDDFT methods for the prediction of linear and nonlinear optical response properties.

The paper is organized as follows. After a short technical outline of the methods used for the calculations, we will discuss the performance of DFT on the electronic spectrum of the title compounds in comparison with highly accurate ab initio data and experimental data. The second part of the paper will be dedicated to the results and performance of TDDFT methods for the calculation of the optical Kerr effect electronic second hyperpolarizability in comparison to experiment and ab initio data. This section is divided into two parts: in the first one, we discuss the properties of the isolated molecules, and in the second part, the possible role of cooperative effects in the condensed phase will be discussed on the basis of dimer calculations.

2. Methods

The excitation spectrum and frequency-dependent response properties have been calculated within the framework of time-dependent density functional theory (TDDFT),[10,11] as recently implemented into the Amsterdam Density Functional program (ADF).[12,13] The response of the system to the external time-dependent electric field is calculated within linear response theory, taking advantage of the $2n + 1$ rule for an efficient analytical calculation of the first hyperpolarizability tensors.[14] Vertical excitation energies are obtained as the poles of the polarizability tensor, the corresponding eigenvalue problem being iteratively solved using the Davidson algorithm for the lowest excitation energies.[10,15,16]

Several different exchange-correlation (xc) potentials have been used. Traditional xc-potentials such as the basic local density approximation (LDA)[17,18] and the generalized gradient approximation (GGA) due to Becke and Perdew (BP86),[19,20] as well as shape-corrected potentials such as LB94 due to van Leeuwen and Baerends,[21] SAOP (statistical average of orbital potentials),[22] and GRAC (BP-LB) (gradient-regulated connection of BP86 and LB94)[23] with correct asymptotic behavior, are employed. Ionization potentials, which are required for GRAC as an input for the specific molecule under study, have been taken from experiment (furan 8.883 eV, thiophene 8.87 eV, selenophene 8.92 eV, tellurophene 8.40 eV)[24−27] for all calcula-

10.1021/jp0208485 CCC: $22.00
Published on Web 09/25/2002

tions. The first-order response of the xc-potential to the external field is described by the so-called xc-kernel. In the current implementation, we use the adiabatic (frequency-independent) local density approximation (ALDA), which can be evaluated efficiently.[12] Previous results suggest that the approximations introduced by using this kernel are less important than those due to the xc-potential.

From the analytically calculated static ($\beta(0;0,0)$) and electrooptical Pockels effect (EOPE, $\beta(-\omega;\omega,0)$) first hyperpolarizability tensor elements, the static ($\gamma(0;0,0,0)$), and the dc Kerr effect (dc-KE, $\gamma(-\omega;\omega,0,0)$) ($\omega = 0.05767$ au $\cong$ 790 nm experimental laser wavelength) have been calculated by finite-field differentiation[28] using external field strengths of $\pm 10^{-4}$ au in the *x*, *y*, and *z* directions. These quantities have been used to estimate the optical Kerr effect (OKE, $\gamma(-\omega;\omega,\omega,-\omega)$) second hyperpolarizabilities via a dispersion relation established by Bishop and Shelton.[29,30] Either a quadratic or a fourth-order fit has been performed using TDDFT values for $\gamma(-\omega;\omega,0,0)$ at two ($\omega = 0$, ω_0; $\omega_0 = 0.05767$ au) or five different frequencies ($\omega = 0$, $\omega_0/4$, $\omega_0/2$, $3\omega_0/4$, and ω_0; $\omega_0 = 0.05767$ au), respectively. The accuracy of the more economic two-point (quadratic) fit has been checked in a few cases, and the results suggest that the latter procedure underestimates the results obtained with the more accurate fourth-order fit only slightly. From the individual γ_{ijkl} tensor elements, the orientationally averaged second hyperpolarizabilities have been calculated using the following formula:

$$\gamma = (\gamma_{xxxx} + \gamma_{yyyy} + \gamma_{zzzz} + 2\gamma_{xxyy} + 2\gamma_{xxzz} + 2\gamma_{yyzz})/5$$

Relativistic effects have been taken into account in an approximate fashion by the scalar-relativistic ZORA (zero-order regular approximation) approach for tellurophene.[31] The influence of relativity has been neglected for the lighter homologues because relativistic effects are expected to be small for these molecules.

Even-tempered basis sets[32] of valence polarized quadruple-ζ/core double-ζ quality plus polarization functions (label QZP) were used in combination with a large fit set.[33] The number of nodeless uncontracted Slater type functions per atom were: H (4s2p1d), C (6s4p2d1f), O (6s4p2d1f), S (8s6p3d1f), Se (10s8p6d2f). For ZORA calculations on tellurophene, a large basis set of polarized quadruple-ζ quality including tight functions was used, which has been designed particularly for accurate relativistic calculations: H (4s2p2d), C (7s4p3d2f), Te (18s14p8d2f). To augment these valence basis sets in the diffuse region, three different basic strategies have been followed and combined with each other to obtain an optimal result. In the first strategy, the valence bases were further augmented in an even-tempered fashion with a set of atom-centered diffuse functions of s, p, d, and f angular momentum (only s, p, d for H). The following basis set labels are used: QZP+*x*d ($x = 0$, 1, 2, 3; i.e., no extra diffuse functions in QZP+0d, one set of diffuse functions (s, p, d, and f type) in QZP+1d, etc.). Particularly to access higher Rydberg excited states, 4s4p4d diffuse nodeless Slater-type basis functions (label MCBF, molecule-centered basis functions) were placed at the geometric center of the five-rings, having the following exponents: s (0.11937, 0.04712, 0.01860, 0.00734), p (0.10782, 0.04256, 0.01680, 0.00663), d (0.07220, 0.02850, 0.01125, 0.00444).[34] Furthermore, atom-centered field-induced polarization functions (label FIP) as proposed by Chong et al.[35,36] have been used together with the valence basis sets described above for hyperpolarizability calculations. Excitation energies have been calculated using the QZP+1d+MCBF basis set, unless stated otherwise.

Very diffuse basis sets such as those used here are likely to cause numerical instabilities due to linear dependencies in the molecular basis set. Linear combinations of basis functions corresponding to small eigenvalues of the overlap matrix ($\leq 10^{-4}$) have therefore been removed from the molecular basis. For example, the following numbers of linear combinations (per symmetry) have been removed from the QZP+1d basis: furan $5a_1+1a_2+0b_1+7b_2$ (351 total, 13 removed), thiophene $5a_1+1a_2+0b_1+7b_2$ (364 total, 13 removed), selenophene: $6a_1+1a_2+0b_1+7b_2$ (394 total, 14 removed), tellurophene $14a_1+5a_2+3b_1+17b_2$ (502 total, 39 removed). The SCF convergence criterion was set to 10^{-10} au, the general integration accuracy parameter used is 6.

Geometries of the individual five-ring molecules were fully optimized in C_{2v} symmetry at the BP86/TZ2P level (ADF basis V), including scalar-relativistic effects (ZORA approach) for tellurophene. The geometries are very close to the experimentally determined data[3] (furan, maximum bond length deviation 0.008 Å; tellurophene, 0.03 Å (Te−C)). All calculations were carried out with the ADF program.[37]

3. Results and Discussion

3.1. Electronic Structure of the Five-Ring Molecules. In this section we will briefly discuss some aspects of the electronic structure of the five-rings to facilitate the interpretation of the valence excitations in the following section. In general, our findings match the results of previous, mainly semiempirical studies; thus we can be short here.[24−27,38,39] Figure 1 shows the three highest occupied and the two lowest unoccupied π-molecular orbitals of the four molecules C_4H_4X (X = O, S, Se, Te), labeled according to C_{2v} symmetry. For all molecules, the 6 π-electrons occupy two levels of b_1 symmetry and one level of a_2 symmetry. The two virtual valence π*-MOs are of a_2 and b_1 symmetry, respectively. Hence, we expect to find six $\pi-\pi^*$ valence excitations in the electronic spectrum, three of which are of A_1 symmetry and another three of B_2 symmetry.

The one-electron energies of the π-states show a characteristic dependency on the heteroatom in the ring. MOs with a nodal plane at the heteroatom, i.e., the two a_2 states, are rather unaffected in energy by the nature of the heteroatom. The two occupied MOs of b_1 symmetry shift to higher energies with the increasing atomic number of the heteroatom. For tellurophene, this eventually leads to a crossover of the two highest occupied MOs, so that the HOMO of tellurophene is of b_1 symmetry, and those of the lighter homologues are of a_2 symmetry. The energy of the LUMO, which is of b_1 symmetry in all cases, is lowered as the heteroatom gets heavier. Given this general electronic structure, one can expect that the electronic excitations of the five-ring molecules will gradually shift to lower energies when going from furan to tellurophene. This will be investigated in some more detail in the following section.

3.2. Electronic Excitation Spectra. The electronic spectra of the furan homologues have been examined by various experimental techniques over the past decades.[24,25,27,39−46] It has been observed that the frequencies of the lowest electronic excitations decrease with increasing atomic number of the heteroatom from furan to the heaviest homologue tellurophene.[27,39] The first quantum chemical calculations of the spectra have been performed many years ago with the main objective to assign the experimentally observed peaks.[24,25,38,39] High-level ab initio calculations using more reliable basis sets and a sophisticated

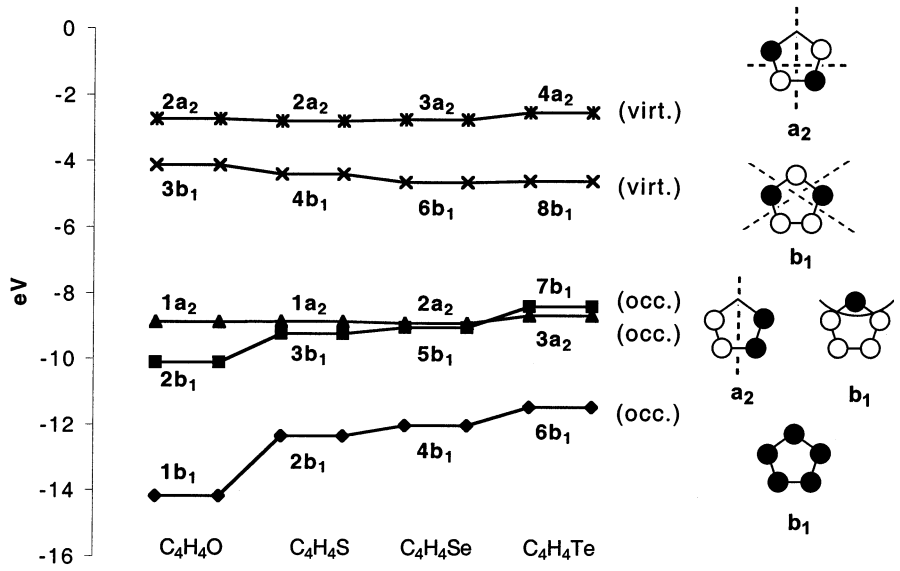

Figure 1. π-levels for the four molecules; GRAC potential, σ-levels not shown.

treatment of electron correlation are currently only available for furan and thiophene. We refer here mainly to the work of Wan et al. using the SAC-CI method,[47,48] the contributions of Serrano-Andres et al. using CASPT2,[49,50] to the studies of Christiansen et al. on furan using the coupled-cluster method,[51,52] to MR-DCI data published by Palmer et al.,[43,53] and to ADC(2) results provided by Trofimov et al.[54] Tozer et al. have reported density functional calculations also for furan and thiophene.[55] For the heavier homologues, selenophene and tellurophene, no ab initio or DFT data are available to date. The comparison of theoretical vertical excitation energies with experimental data, on the other hand, bears some difficulties, as has been elaborated recently by Christiansen et al. for one of the title compounds.[51] This has to be taken into account when the performance of our results is judged by comparison with experiment for selenophene and tellurophene.

In this section, we discuss the performance of the current TDDFT methods for the prediction of the lowest excitations of the title compounds by comparison with currently available reference data. The results will give an indication about the accuracy of current density functional methods in the prediction of optical properties and will furthermore aid in the rationalization of the nonlinear optical properties reported subsequently. We limit ourselves here to the lowest few excitations, which are usually the most important ones for these properties. We begin with the discussion of the valence $\pi-\pi^*$ excitations for each of the four molecules and deal with the Rydberg excitations in the second part of this section. The results will be summarized before we go on to the second hyperpolarizabilities.

3.2.1. Valence ($\pi-\pi^*$) Excitations. Furan. From the general electronic structure discussed before, we expect six $\pi-\pi^*$ excitations, of which only the lowest four will be discussed here, in accordance with previous theoretical studies. Table 1 shows the four lowest electronic excitations of furan as calculated with different xc-potentials, together with the results from previous studies. The lowest $\pi-\pi^*$ excitation is of B_2 symmetry and contains a dominant contribution from the HOMO−LUMO transition ($1a_2 \rightarrow 3b_1$). The second and third lowest $\pi-\pi^*$ excitations, which are of A_1 symmetry, can both be represented by a mixture of $1a_2 \rightarrow 2a_2$ and $2b_1 \rightarrow 3b_1$ orbital replacements. The highest B_1 excitation in Table 1 usually has high $2b_1 \rightarrow 2a_2$ character. The two remaining valence $\pi-\pi^*$ excitations come at higher energies and are not discussed here.

TABLE 1: Furan Valence ($\pi-\pi^*$) Excitations (eV)

method	B_2	A_1	A_1	B_2
LDA	5.87	6.27	7.41	8.22
BP86	5.82	6.30	7.40	8.18
GRAC	5.96	6.30	7.84	8.29
SAOP	5.99	6.32	8.03	8.48
LB94	5.97	6.15	7.97	8.41
HCTH(AC)	6.08	6.42	8.16	
CASPT2	6.04	6.16	7.74	8.38
MRMP	5.95	6.16	7.69	
ADC(2)	6.37	6.70	8.16	8.64
SAC−CI	6.40	6.79	8.34	9.08
CC3	6.35	6.61	8.35	9.09
MR-DCI	6.88	6.63	9.36	9.48
exp	5.88[a] 6.01[b]	6.48[a]		

[a] Reference 44. [b] Reference 39.

The excitation energies obtained for the two lowest valence excitations are generally rather similar with all xc-potentials studied here. LDA and BP energies lie about 0.1 eV lower than those of GRAC, SAOP, and LB94 for the lowest B_2 excitation ($1B_2$). Also, for $1A_1$, all potentials yield the same excitation energy within 0.05 eV, with the exception of LB94, which is 0.15 eV lower in this case. Somewhat greater differences appear for the second lowest excitations of each symmetry ($2A_1$ and $2B_2$). In each case, the GRAC value is bracketed by the lower values of LDA and BP and the higher values of SAOP and LB94.

On comparison with results from ab initio methods, our present DFT energies match best with multireference perturbation theory based methods (CASPT2 and MRMP). The latter methods produce excitation energies within 0.1 eV deviation from each other and tend to be on the low-energy side of the ab initio theoretical predictions. CC3 and SACCI produce similar values at rather higher energies, as does ADC(2). MRDCI generally predicts the highest excitation energies (with the exception of $1A_1$, where SACCI takes the top). A fair comparison of the accuracy of the different methods and our present DFT results is difficult partly due to the different basis sets used, but we dare conclude that the DFT methods, especially GRAC and SAOP, are not very much inferior to sophisticated ab initio methods in this case. The GRAC potential, like HCTH(AC), connects a GGA potential in the interior of the molecule (BP in the case of GRAC) to a $-1/r$ type asymptotic

TABLE 2: Thiophene Valence ($\pi-\pi^*$) Excitations (eV)

method	B_2	A_1	A_1	B_2
LDA	5.56	5.53	7.03	7.09
BP86	5.58	5.57	7.06	7.16
GRAC	5.57	5.56	6.98	7.16
SAOP	5.60	5.55	7.13	7.17
LB94	5.51	5.38	7.00	6.97
HCTH(AC)	5.65	5.64	7.35	7.34
CASPT2	5.72	5.33	6.69	7.32
SAC−CI	5.72	5.41	7.32	7.40
MR-DCI	6.00	5.69	7.91	8.10
exp	5.19[a]	5.83[a]		
	5.26[b]	5.64[b]		
	5.16[c]	5.99[c]		

[a] Reference 44. [b] Reference 39. [c] Reference 45.

TABLE 3: Selenophene Valence ($\pi-\pi^*$) Excitations (eV)

method	B_2	A_1	A_1	B_2
LDA[a]	5.33	5.14	6.85	6.76
BP86[a]	5.34	5.17	6.87	6.85
GRAC	5.33	5.16	6.80	6.85
SAOP	5.35	5.13	6.89	6.82
LB94	5.26	4.96	6.74	6.63
exp	5.33[b,d]	5.05[b,d]		
	5.4[c]	4.92[c]		

[a] QZP+1d basis (without MCBF). [b] Reference 44. [c] Reference 39. [d] Reference 46.

part. For the lowest two excitations, HCTH(AC) yields excitation energies some 0.1 eV above those of GRAC, whereas a larger deviation shows up for the second lowest A_1 excitation. To our experience, limitations in the basis sets tend to produce higher excitation energies, especially for the higher-lying excitations. Hence, the difference between our DFT results and those of Tozer et al. probably lie within the margin of the different basis sets used. Moreover, our DFT calculations compare reasonably well with experimental excitation energies, although a direct comparison is not always straightforward.[51]

Thiophene. In general, similar conclusions as for furan can be drawn from a comparison of the lowest valence excitation energies in thiophene (Table 2). Here, GRAC appears similar to LDA and BP, SAOP generally yields slightly higher excitation energies, and LB94 energies are found on the low-energy side. Although fewer ab initio results are available for thiophene than furan, similar conclusions can be drawn also here. The DFT results lie on the low-energy range of the theoretical predictions, and the best overall agreement is found with CASPT2. An exception is marked by the $2A_1$ excitation, which appears at a conspicuously low energy within the CASPT2 scheme. Here, our results compare better with the SACCI energy. In general, the agreement between DFT and ab initio predictions is somewhat better for thiophene than for furan. Experimental excitation spectra suggest a considerably lower excitation energy for the lowest B_2 state than all the theoretical methods, whereas the opposite is true for the lowest A_1 valence excitation.

Selenophene, Tellurophene. For the heavier homologues selenophene (Table 3) and tellurophene (Table 4), we can only compare our DFT values to a small number of experimentally identified transitions. No ab initio calculations of the electronic excitation spectrum of these compounds are available to date.

Even more here than for the lighter homologues, all the DFT methods yield very similar valence excitation energies. LB94 again marks the low end of the excitation energy spectrum for both selenophene and tellurophene. Within the limitations stated

TABLE 4: Tellurophene Valence ($\pi-\pi^*$) Excitations (eV)

method	B_2	A_1	A_1	B_2
LDA[a]	5.03	4.48	6.51	6.09
BP86[a]	5.05	4.51	6.57	6.17
GRAC	5.04	4.50	6.54	6.12
SAOP	5.07	4.44	6.58	6.10
LB94	4.98	4.28	6.46	5.96
exp	5.12[b,c]	4.44[b,c]		5.95[c]
	5.35[b,d]			

[a] QZP+1d basis (without MCBF). [b] Reference 44. [c] Reference 39. [d] Not assigned in ref 44.

TABLE 5: Lowest Valence ($\pi \rightarrow \pi^*$) Excitations for C_4H_4X; GRAC/QZP+1d (eV)

X	B_2	A_1	A_1	B_2
O	5.96	6.30	7.84	8.29
S	5.57	5.56	6.98	7.16
Se	5.33	5.16	6.80	6.85
Te	5.04	4.50	6.54	6.12

before, we can say that the agreement between DFT and experiment is very good (reproduction within 0.2 eV). Scalar relativistic effects, which have been included in the calculations for tellurophene by the means of the ZORA approach, have only minor effects on the excitation energies (data not shown). For instance, they increase the excitation energy of the lowest two excitations in all xc-potentials but have little effect on the third and fourth excitation.

Influence of the Heteroatom. Table 5 collects the results for all furan homologues as computed by the GRAC potential to illustrate the influence of the heteroatom on the lowest valence excitation energies. Similar numbers and trends are predicted by the other xc-potentials, as can be judged from the tables for the individual molecules.

As can already be expected from the change in orbital energy differences reported before (cf. Figure 1), the electronic excitations generally decrease with increasing atomic number of the heteroatom X in C_4H_4X. This effect is most pronounced for the lowest A_1 excitation in the five-rings, which decreases by 1.8 eV (GRAC) from 6.3 eV in furan to 4.5 eV in tellurophene. The decrease in the lowest excitation of B_2 symmetry ($a_2 \rightarrow b_1$ excitation) is more modest and amounts to only 0.9 eV. Hence, although the lowest excitation energy is of B_2 symmetry in furan, the lowest excitations in both symmetries appear at very similar energies in thiophene, and A_1 is the symmetry of the lowest excitations in selenophene and tellurophene. For the second-lowest valence excitations of each symmetry ($2A_1$ and $2B_2$), the opposite trend is observed in the sense that $2B_2$ is much more sensitive to the influence of the heteroatom that $2A_1$. It should be noted here that these trends can be rationalized on the basis of the heteroatom dependence of the orbital energies as shown in Figure 1.

3.2.2. Rydberg Excitations. In this section, we deal with the Rydberg excitation energies of the five-ring molecules and highlight the different performance of xc-potentials in comparison to ab initio data for furan and thiophene. Due to the lack of reliable reference data, our DFT results for selenophene and tellurophene are excluded from the discussion. The DFT excitations have been classified qualitatively into Rydberg and valence excitations on the basis of the shapes and size of the orbitals involved. On the basis of this assignment, corresponding Rydberg-type excitations from our DFT and ab initio calculations have been juxtaposed in Tables 6 and 7. Note that this assignment is only qualitative in nature. Very often, though, the relative energy orders of the states coincide for DFT and

TABLE 6: Furan Rydberg Excitations (eV)

label	SAOP	GRAC	SACCI[47]	CC3[52]	CASPT2[49]	MRDCI[53]	ADC(2)[54]	MRMP[64]	HCTH(AC)[55]
$1A_2$ s	6.12	5.69	5.99	5.96	5.92	5.95	5.86	5.84	5.93
$1B_1$ *y*	6.76	6.24	6.45	6.50	6.46	6.63	6.35	6.40	6.54
$2A_2$ *z*	6.90	6.38	6.66	6.65	6.59	6.41[a]	6.50	6.53	6.60
$3A_2$	7.17[c]	6.80[c]	7.04	7.12[b]	7.00	7.15[a]	6.89	6.98	6.98
$2B_1$ *yz*	7.33	6.86	7.14	7.18	7.15	6.99	6.98	7.10	7.14
$2B_2$ *x*	7.41	6.93	6.82	6.82	6.48	6.66	6.73	6.50	6.78
$3B_1$ s	7.47	6.93	7.45	7.36	7.21	7.14	7.05	7.31	7.20
$4A_2$ z^2	7.59[c]	7.21[c]	7.27	7.26	7.22	7.41	7.11	7.18	7.20
$3A_1$ *xy*	8.31	7.74	7.36	7.44	7.31	7.75	7.22	7.26	7.40
$3B_2$ *xz*	8.64	7.97	7.51	7.60	7.13	7.71[a]	7.35	7.18	7.47

[a] Reference 52. [b] Reference 47. [c] Not very firm assignment.

TABLE 7: Thiophene Rydberg Excitations (eV)

label	SAOP	GRAC	SACCI[48]	CASPT2[50]	MRDCI[43]	HCTH(AC)[55]
$1A_2$ s	6.16	5.68	5.70	5.93	5.78	5.94
$2B_1$ s	6.46	6.04	6.12	6.23	6.33	6.32
$3A_2$ *z*	6.93	6.41	6.41	6.58	7.03	
$3B_1$ *y*	6.95	6.36	6.47	6.30	6.41	6.72
$4A_2$ d+2	6.99	6.60	6.73	6.97		6.91
$6A_2$ *y*	7.26	6.74	6.89	6.35	6.39	6.59
$4B_1$ *z*	7.27	6.76	6.73	6.83	7.18	
$5A_2$ $x^2 - y^2$	7.32	6.91	6.75	7.08	7.85	7.07
$5B_1$ z^2	7.39	7.00	7.14	7.37		
$2B_2$ *x*	7.41	6.80	6.41	6.56	7.10	6.74
$3A_1$ *x*	7.75	7.28	6.73	6.76	7.31	
$4A_1$ *xy*	8.34	7.68	7.08	7.23	7.93	7.45
$3B_2$ *xz*	8.35	7.65	7.12	7.28	7.76/8.11	7.43

ab initio; i.e., the lowest states found with the different ab initio methods are also the lowest states in DFT. Our discussion focuses on the shape-corrected potentials SAOP and GRAC, which exhibit a correct asymptotic long-range behavior and can thus be expected to provide a reasonable description of Rydberg states, which are very diffuse in nature. In Tables 6 and 7, corresponding excitations to Rydberg states are tabulated for furan and thiophene, respectively.

As a general trend, the TDDFT excitation energies of furan obtained using the traditional LDA and BP potentials (data not shown) are usually considerably too low in comparison with available reference data (up to 1 eV). Likewise, the asymptotically correct LB94 potential delivers transition energies that are generally too high (up to 1 eV). The excitation energies calculated within SAOP and GRAC are usually within or close to the range given by the various ab initio methods (Tables 6 and 7). The SAOP potential tends to overestimate excitations a bit.

For most of the 10 lowest Rydberg excitations in furan, the GRAC potential yields excitation energies that are often just slightly lower than the predictions made by ab initio methods (about 0.2 eV). Exceptions to this rule mark the Rydberg-p_x ("$2B_2$") excitation and the highest two excitations reported here, where the GRAC numbers are somewhat higher than the reference data, although some uncertainties remain in the assignment of these excitations. Unlike the observations with the valence excitations, the agreement between different ab initio methods is rather good (usually within 0.2−0.3 eV). Again, CASPT2 and MRMP on one hand, and CC3 and SACCI on the other hand, yield very similar values. Note, however, that the spread does increase for higher excitations. SAOP invariantly yields values substantially higher than GRAC and the other methods (about 0.5 eV, up to 1 eV). Similar results are obtained for thiophene (Table 7). Here, the GRAC values usually fall within the range of the ab initio values; i.e., the latter sometimes yield higher, sometimes lower values than GRAC. Again, the SAOP Rydberg spectrum seems to be shifted up in energy, giving overestimated Rydberg excitation energies.

The different performance of xc-potentials, especially SAOP and GRAC, for Rydberg excitations may be rationalized by considering the different shape of these potentials. The energy of the Rydberg states (or orbitals), which are very diffuse, is determined by the asymptotic region of the xc-potential. Both SAOP and GRAC have the proper Coulombic (1/*r*) asymptotics, so the Rydberg states are determined by a potential of similar shape in both cases. Hence, one can expect that they appear at approximately the same energy in both xc-potentials. The shape of SAOP and GRAC differ, however, at intermediate distances from the nearest nucleus, in a region of strong influence on the highest occupied orbitals. For the exact Kohn−Sham-potential, the orbital energy of the HOMO is equal to the negative of the ionization potential of the molecule.[56,57] Within the SAOP approximation, the orbital energy of the HOMO is somewhat too low (by about 0.5 eV in furan), i.e., the exact (experimental) ionization potential is overestimated. Because the valence orbitals are all determined by more or less the same region of the xc-potential, the error cancels largely for valence excitations, but not so for Rydberg excitations, where the initial and final states of the excitation are dominated by different regions of the xc-potential. The GRAC potential is less sensitive to this error, because the exact (experimental) ionization energy of the molecule enters the potential as a parameter. To compare the approximate GRAC and SAOP potentials, one can uniformly shift the orbital spectrum resulting from both potentials in a way that the orbital energy of the HOMO matches the experimental ionization energy in both cases. In doing so, it becomes apparent that the highest occupied and the lowest few unoccupied orbitals have similar absolute energies for both potentials. In contrast, the energies of the higher unoccupied orbitals are somewhat higher for SAOP (up to approximately 1 eV) than the corresponding GRAC energies. In other words, the energy gap between the outer and valence regions is higher for SAOP than for GRAC, making SAOP less attractive in the outer region compared to the valence region. This trend in the one-electron energies is reflected in the Rydberg excitations reported above, which are computed at higher energies with SAOP than with GRAC.

In summary, all the potentials studied here perform very similarly for the lowest valence excitations, and modest differences arise for the higher excitations. Presumably for the same reasons, significant differences show up for excitations to Rydberg states: Rydberg excitations are generally too high within SAOP and LB94, too low with LDA and BP86, but only very slightly too low for GRAC. These observations can be rationalized by considering the shape characteristics of the various xc-potentials and by inspection of the orbital energy spectrum. The absolute accuracy of the current DFT excitation energies is difficult to judge in this case, because even results derived from sophisticated ab initio methods differ considerably.

The DFT results appear to be in error by about 0.2−0.3 eV, which is an accuracy that is comparable to the more expensive ab initio methods.

3.3. Second Hyperpolarizabilities $\gamma(0;0,0,0)$ and $\gamma(-\omega;\omega,\omega,-\omega)$. The orientationally averaged isotropic second hyperpolarizability of the furan homologues has been measured by Kamada et al. using a femtosecond optical-heterodyne-detected optical Kerr effect (OHD-OKE) experiment, employing an incident laser wavelength of 790 nm.[4,5] The electronic second hyperpolarizability has been separated from the vibrational component by making use of the faster response time of the former. Hence, theoretical calculations of the electronic second hyperpolarizability can be directly compared to the experimental values. The experimental data show a strong influence of the heteroatom on the observed second hyperpolarizability, increasing the property from 15 500 au for furan to 75 100 au for the heaviest analogue, tellurophene.[5] The same authors have performed theoretical calculations on the static second hyperpolarizability of the same molecules using a selection of ab initio methods and basis sets.[4,6,7] The most sophisticated method used is the CCSD(T) model in combination with Gaussian basis sets including diffuse functions. Although the static values provided by these calculations are in good agreement with the experimental frequency-dependent values for furan and thiophene, the property is severely underestimated for the heavier homologues, especially for tellurophene. The discrepancy for the latter is as much as 48% (38 800 au for CCSD(T) vs 75 100 au for the experiment), despite the quite sophisticated correlation treatment employed.

The matter of frequency dispersion was addressed by Millefiori et al.[8] and by Ohta et al.[7] at the time-dependent Hartree−Fock level of theory. A dispersion enhancement for $\gamma(-\omega;\omega,\omega,-\omega)$ of 22−33% was found on going from zero frequency to the experimental laser frequency. Due to the lack of electron correlation, the absolute values obtained with this method are poor, however. In the same paper, Millefiori et al. present density functional calculations on the static second hyperpolarizability $\gamma(0;0,0,0)$ of the five-rings using three different density functionals (BLYP, B3LYP, MPW1PW91). Their results show that BLYP overestimates the reference static CCSD(T) value, whereas MPW1PW91 underestimates the property. B3LYP seems to give the best accuracy (with respect to the CCSD(T) reference value) within the density functional methods studied in this paper. The large disagreement for the heavier homologues of furan could not fully be clarified by these theoretical studies, however. Kamada et al. have discussed basically three different explanations for the observed differences between calculated values at that time and experimental data, which are: (1) frequency dispersion, (2) basis set deficiencies, and (3) relativistic effects.[6] On the basis of their TDHF calculations, Millefiori et al. disfavor frequency dispersion as the main source of error in the theoretical calculations.

In the present study, we extend the recently reported theoretical results by TDDFT calculations for the static and frequency-dependent second hyperpolarizabilities using five different exchange-correlation potentials, including shape-corrected potentials that have been designed especially for (hyper)-polarizability calculations. For the purpose of the present study, the static CCSD(T) values provided by Kamada et al. serve as a benchmark for our static DFT values $\gamma(0;0,0,0)$ of the isolated five-ring molecules. The frequency-dependent DFT estimates for the OKE effect $\gamma(-\omega;\omega,\omega,-\omega)$, which were calculated at the experimental laser frequency ($\omega = 0.0577$ au), are compared to the experimental values directly. The effect of frequency dispersion as estimated on the basis of the present TDDFT calculations is compared to the TDHF values provided by Millefiori et al.

TABLE 8: Diffuse Basis Sets for $\gamma(0;0,0,0)$ and $\gamma(-\omega;\omega,0,0)$ ($\omega = 0.0577$ au) for Furan and GRAC (au)

basis set	basis functions removed/total[a]	$\gamma(0;0,0,0)$	$\gamma(-\omega;\omega,0,0)$
V	0/189	4777	5135
QZP	1 + 0 + 0 + 3 = 4/300	7822	8467
QZP+FIP	9 + 2 + 1 + 10 = 22/388	12930	14390
QZP+1d	5 + 1 + 0 + 7 = 13/351	12110	13400
QZP+1d+MCBF	9 + 2 + 1 + 10 = 22/387	12950	14340
QZP +1d+FIP	18 + 6 + 4 + 23 = 51/467	12660	14060
QZP+2d	14 + 6 + 2 + 21 = 43/467	12930	14270
QZP+2d+MCBF	23 + 8 + 6 + 26 = 63/503	13940	15330
QZP+2d+FIP	31 + 12 + 8 + 39 = 90/583	12950	14340
QZP+2d+FIP+MCBF	34 + 14 + 9 + 42 = 99/619	12410	13550

[a] Removed functions in symmetry species $a_1 + a_2 + b_1 + b_2$ = total removed/total number of original basis functions.

3.3.1. Basis Set Saturation Study. Before presenting the performance of xc-potentials, we summarize the results of our basis set study. Basis set insufficiencies have been mentioned in previous studies as one of the possible origins for the large discrepancies between experiment and theory. The basis sets used in this study are of double-ζ quality in the core region and of quadruple-ζ quality in the valence space (cf. section 2). We assume that this is close to the basis set limit for the core and valence regions.[58] Hence, we focus on the effects of basis set augmentation in the diffuse regime. Moreover, we restrict our report here to the results for furan, because similar basis set trends can be expected for the higher homologues. In fact, agreement has been checked for a few selected cases.

We have basically followed three different strategies to tackle the diffuse basis set region (see methods section 2). The most straightforward and systematic choice is an even-tempered extension of the atom-centered basis set (QZP+*x*d, $x = 0, 1, 2, 3$, cf. section 2). However, extensive test calculations (details not shown here) indicate that this augmentation strategy is not the best choice to push to the basis set limit. Especially for the traditional xc-potentials LDA and BP86, no converged value for the second hyperpolarizability was reached up to QZP+3d. This is accompanied by increasing dependency problems due to strong overlap of very diffuse atom-centered basis functions. Better results were obtained using basis sets that were augmented by molecule-centered basis functions (MCBF) and by field-induced polarization functions (FIP), as collected in Table 8 for the GRAC potential. In the same table, information is provided about how many basis functions are taken away from the molecular basis to avoid strong dependencies.

As can be seen, most of the different strategies yield similar second hyperpolarizabilities (variance about 10%), although they contain different numbers and kinds of diffuse basis functions. As expected, valence-only basis sets without augmentation in the diffuse region are inappropriate for the computation of this property (Table 8, entries V and QZP). We conclude from our results that a static hyperpolarizabilty of furan of approximately 12 900 au is close to the value at the basis set limit, which is approached, among others, by the QZP+2d basis set. On the other hand, even the more economic basis QZP+1d approaches the limit within 5%. Moreover, using this basis set, only rather few functions have to be removed from the overall molecular basis to fulfill the dependency criterion. From extensive test calculations using even-tempered basis sets (not shown), we can conclude that the results of this basis set study can safely be transferred to other xc-potentials and molecules.

TABLE 9: $\gamma(0;0,0,0)/\gamma(-\omega;\omega,\omega,-\omega)$ ($\omega = 0.0577$ au) for Different xc-Potentials in Basis QZP+1d (au)

γ(static)/ γ(OKE)	furan	thiophene	selenophene	tellurophene
LDA	13850/17090	20430/25200	25430/31760	38420/51900[b]
BP86	13600/16830	19190/23570	26300/32700	38260/52060[b]
GRAC[a]	12110/14680	18470/22570	23760/29470	39290/53440[b]
SAOP	8969/10570	13750/16280	17740/21310	27500/35540[b]
LB94	7279/8424	11560/13450	14420/16990	20910/26060[b]
CCSD(T) (static)	14750/- - -	19990/- - -	25460/- - -	38800/- - -
expt (OKE)	- - -/15500	- - -/26200	- - -/34500	- - -/75100

[a] Experimental IP used throughout. [b] Results using the less accurate quadratic fit to estimate the frequency dispersion contribution for tellurophene: 50540 (LDA), 50600 (BP86), 52010 (GRAC), 34890 (SAOP), 25540 (LB94).

3.3.2. Performance of xc-Potentials. Table 9 shows the static and OKE second hyperpolarizabilities of furan and its heavier homologues thiophene, selenophene, and tellurophene as calculated in this study with different xc-potentials, together with CCSD(T) and experimental benchmark values. As already found in previous calculations reported in the literature, we observe an increase of the second hyperpolarizability with the atomic number of the group 16 heteroatom as a general characteristic reproduced by all xc-potentials. The absolute values calculated with different xc-potentials, however, vary considerably within up to 50% for a given molecule. Within the standard QZP+1d basis set, the second hyperpolarizabilities calculated with the LDA and BP86 potentials generally yield the best match with the CCSD(T) reference for all molecules. This may come as a surprise if one considers results for very small molecules,[59] where LDA and GGA lead to systematic overestimations by approximately a factor of 2. A partial explanation is given by the reduced importance of the outer region for larger molecules. The similar performance of LDA and BP suggests that gradient corrections are not of prime importance for the property studied here. xc-potentials with asymptotically correct behavior usually yield somewhat lower values than LDA or BP86. LB94 invariantly underestimates γ severely by almost a factor of 2. SAOP is somewhat better but still is systematically too low. GRAC slightly underestimates the CCSD(T) value by 5−15% for furan, thiophene, and selenophene, whereas it matches the reference for tellurophene very closely. In section 3.3.5, the different performance of the various xc-potentials studied here will be related to the corresponding excitation spectra.

3.3.3. Frequency Dispersion. Experimental measurements of the EOPE of the furan homologues have been performed using the OHD-OKE technique, with the wavelength of the incident laser radiation 790 nm (frequency $\omega = 0.0577$ au). Static second hyperpolarizability values are not directly accessible by experiment. Using an approximate dispersion relation and our TDDFT values for $\gamma(-\omega;\omega,0,0)$ (cf. section 2), a relative increase in $\gamma(-\omega;\omega,\omega,-\omega)$ of 21−36% (GRAC potential) at the experimental frequency compared to the static value $\gamma(0;0,0,0)$ (Table 9) has been found. The effect of frequency dispersion has been studied at the TDHF level for these molecules before,[7,8] and a similar increase in γ has been found (22−33%). No correlated ab initio frequency-dependent second hyperpolarizabilities are available for these molecules up to now. However, Kamada et al. used an approximate dispersion scaling scheme using the TDHF dispersion contribution to correct the static CCSD(T) values obtained earlier. Using this scheme, an overestimation of the OKE effect is obtained for furan, whereas the scaled value for tellurophene is still underestimated by 31% (51 690 au vs 75 100 au).[7]

The limited frequency dispersion contribution predicted by our TDDFT calculations and the ab initio results available so far can be rationalized by the fact that the frequency of the incident laser radiation is considerably lower than the lowest resonance frequency for electronic excitation of the furan homologues. Tellurophene shows the lowest electronic excitations of all homologues, and hence, the frequency dispersion enhancement increases from furan to tellurophene. However, the modest increase confirms the earlier suggestion that frequency dispersion cannot alone be held responsible for the exceptionally high second hyperpolarizability of tellurophene as measured experimentally.

TABLE 10: Scalar Relativistic Effect on the Second Hyperpolarizability of Tellurophene Using the ZORA Approach; $\gamma(0;0,0,0)/\gamma(-\omega;\omega,0,0)$ (au)

$\gamma(0;0,0,0)/$ $\gamma(-\omega;\omega,0,0) \rightarrow$	nonrelativistic	scalar ZORA
LDA	39400/45700	40600/47200
BP86	34300/39700	38300/44400
GRAC	38740/44950	39290/45640
SAOP	27200/30800	27500/31100
LB94	20700/23000	20900/23200

3.3.4. Relativistic Effects. The influence of relativity on the second hyperpolarizability has been included in an approximate fashion using the scalar-relativistic ZORA approach for tellurophene, using a specially optimized quadruple-ζ basis set with tight core functions and even-tempered diffuse functions (section 2). Relativistic effects should be small for the lighter homologues and have thus not been studied here. Table 10 indicates the change in $\gamma(-\omega;\omega,0,0)$ and $\gamma(0;0,0,0)$ for tellurophene using the scalar ZORA approach and nonrelativistic calculations for different xc-potentials. It can be seen that scalar ZORA, with the exception of the BP86 values, only leads to a very slight increase of the second hyperpolarizabilities for these molecules. Relativistic effects can thus not be held responsible for the difference between theoretical calculations and experimental data.

3.3.5. Discussion: Second Hyperpolarizabilities and Excitation Spectra. The (hyper)polarizability of any molecule can be expressed by an appropriate sum-over-states (SOS) formula[60,61] and is thus closely related to the electronic excitation spectrum of the molecule. For example, for the diagonal component:

$$\gamma_{iiii}(0;0,0,0) = 24\sum_{n\neq g}\left[\frac{(\mu^i_{ng}\Delta\mu^i_{ng})^2}{(\Delta E_{ng})^3} - \frac{(\mu^i_{ng})^4}{(\Delta E_{ng})^3} + \sum_{m\neq n,g}\frac{(\mu^i_{ng}\mu^i_{nm})^2}{\Delta E_{mg}(\Delta E_{ng})^2}\right]$$

μ^i_{ng} = transition dipole moment in direction i

$\Delta\mu^i_{ng}$ = change in dipole moment along direction i upon excitation

ΔE_{ng} = excitation energy from ground state g to state n

We use this relation here to link the results obtained for the second hyperpolarizabilities and the excitation energies in a qualitative manner. This is particularly important because the experimental excitation energy spectra of all the five-ring heterocycles are reasonably well reproduced by the theoretical calculations, whereas large differences between theory and experiment remain for the second hyperpolarizabilities. We will show here and in the next section that this is not likely due to a shortcoming in the theoretical approaches but may be related to a different origin like intermolecular interactions or condensed phase effects.

Considering the SOS formula, it is clear that the second hyperpolarizability will get its largest contributions from the lowest energy electronic transitions, and from those with the largest oscillator strengths. Experience from SOS calculations of first hyperpolarizabilities suggests, however, that sometimes quite many excited states have to be taken into account to get the property converged. Moreover, it is not always a priori clear whether inclusion of a certain state will increase or decrease the property value. As a consequence, there is no "variational principle" for the second hyperpoarizability, so that a better basis set need not *necessarily* increase the value. However, we can assume that the *qualitative* trends can be understood on the basis of the lowest few excitations which we have reported earlier.

As demonstrated above, the lowest *valence* ($\pi \rightarrow \pi^*$) excitation energies are reproduced by all xc-potentials with rather uniform quality, suggesting that the origin of the deviations in performance for second hyperpolarizabilities is not rooted here. A significant dependence on the xc-potential used has been established for the Rydberg excitations, however. The rather largely differing performance of GRAC on one hand and SAOP (also LB94) on the other hand is of special interest to us. Although the average oscillator strength for excitations calculated with SAOP is even slightly higher than that for GRAC (data not shown here), it has been shown that the Rydberg excitations appear at considerably higher energy for the former potential. Hence, the contribution of the Rydberg states to the second hyperpolarizability is underestimated by SAOP, leading to the low overall result. Similar arguments hold for LB94. On the other hand, the seemingly good performance of LDA and BP must be attributed to fortuitous error cancellation. Rydberg states are predicted at too low energies within these potentials. However, the oscillator strengths of the corresponding excitations are likewise underestimated with respect to GRAC, for instance. Hence, considering the SOS formula given above, it is understandable why good overall results may be obtained with these potentials as well.

The stability/instability of certain xc-potentials with respect to an increase in basis set diffuseness as reported in section 3.3.1 can also be recognized in the changes in the corresponding excitation spectra. Within the BP86 potential, even the lowest excitation energies are substantially lowered when more diffuse basis functions are added. Conversely, the basis set dependence of the excitations calculated with GRAC shows a more physical behavior. Here, the lowest excitations are barely affected by the presence or absence of diffuse functions. As expected, only the higher excitations occur at lower energy when more diffuse functions are added. Hence, calculations of (hyper)polarizabilities in very diffuse basis sets tend to be overestimated by LDA and BP86, whereas the asymptotically correct potentials show better convergence with basis set size.

3.3.6. Bulk Effects: Dimers. The results presented in the previous sections show that DFT results are in reasonable agreement with recent CCSD(T) calculations for the static second hyperpolarizability for all molecules. However, when the theoretical values are compared with experimental data, there still is a problem with the heavier five-rings, in particular with tellurophene, which has not been directly resolved by any of the theoretical studies presented so far. Previously, three possible reasons for the discrepancy between calculated and experimental values were discussed. Here, we have demonstrated that none of them can fully explain the deviation from experiment.

When experimental data (OHD-OKE experiment) are compared, one should bear in mind that the measurements have been performed in the liquid state, that is each individual molecule has a number of neighbors in its close vicinity, which are likely to have influence on its electronic properties (cooperative effects). The calculations presented so far here and in the literature only deal with isolated molecules in the gas phase. This situation is only comparable to the experimental conditions if there were no or only insignificantly weak interactions between the individual molecules. Given the deviations between calculations and experiment described in the previous sections, we now investigate the influence of intermolecular interactions on the molecular second hyperpolarizability by studying a dimer of molecules instead of an isolated monomer. This can be considered as a very first step to model the situation in the condensed phase. Clearly, for a full study of the hyperpolarizability of the liquid within a supramolecular approach, many configurations and cluster sizes have to be included and, also already on the dimer stage, a thermal averaging over different conformations has to be done. This is, however, outside the scope of the present study. Instead, as a first approximation we here include only a single dimer configuration to show how the second hyperpolarizability is likely to change on going from isolated molecules in the gas phase to aggregates that may (at least temporarily) be formed in the liquid. The dimer configuration we have chosen is depicted in Figure 2. Other configurations have also been considered, but they appear to result in a less effective packing of the molecules in the condensed phase. For instance, a "parallel" C_{2v} dimer configuration (cf. the "antiparallel" C_{2h} configuration illustrated in Figure 2) favors larger interplane distances due to repulsion of the bulky tellurium centers, which is reduced in the "antiparallel" orientation shown in Figure 2.

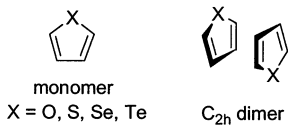

Figure 2. C_{2h} dimer configuration.

Assuming the structural model depicted in Figure 2 as a simple parallelepiped, the distance between the planes of the five-rings in the liquid can be estimated from the experimental densities of the liquids,[62] the optimized monomer geometries, and the van der Waals radii[63] of the peripheral atoms to roughly 3.2 Å for furan, 3.0 Å for thiophene and selenophene, and 2.8 Å for tellurophene. These plane distance estimates are slightly smaller than the van der Waals distance of two carbon atoms (3.4 Å), and fall well below all X−X van der Waals contacts except O−O (X = S, Se, Te; van der Waals radii: H 1.20 Å, C 1.70 Å, O 1.52 Å, S 1.80 Å, Se 1.90 Å, Te 2.06 Å).[63] The effect of aggregation on the hyperpolarizabilities should be larger for smaller distances, an expectation that is also confirmed by our calculations (see below). To obtain a conservative estimate on the effect of dimer formation, we have constructed model dimers as shown in Figure 2 from the monomer geometries, featuring 4.0 and 3.5 Å interplane distances without further geometry optimization. Table 11 shows the second OKE hyperpolarizability $\gamma(-\omega;\omega,\omega,-\omega)$ *per molecule* in these dimers in comparison with the monomers and the experimentally obtained values.

The calculated molecular second hyperpolarizability increases considerably upon dimer formation, the largest gain being observed for tellurophene, where the experimental value is approached within 10% or better, depending on the plane distance used. The DFT value for the furan dimer overshoots the experimental value somewhat, whereas the values obtained for the thiophene and selenophene match the experimental data

TABLE 11: $\gamma(-\omega;\omega,\omega,-\omega)$[a] per Molecule; GRAC/QZP+1d (au)

		dimer		
	monomer	$d = 4.0$ Å[b]	$d = 3.5$ Å[b]	experiment
furan	14680	16820	17140	15500
thiophene	22570	24520	25080	26200
selenophene	29470	32330	33640	34500
tellurophene	53440	62520[c]	69320[c]	75100

[a] Quadratic fit used to estimate frequency dispersion contribution. [b] Interplane distance. [c] Results from fourth-order frequency dispersion fit: 66700 ($d = 4.0$ Å), 74190 ($d = 3.5$ Å).

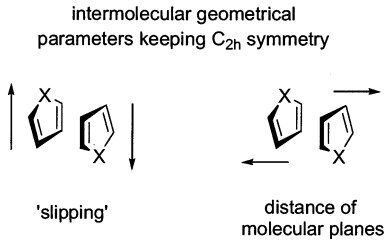

Figure 3. Geometrical degrees of freedom within C_{2h} symmetry.

quite closely. In summary, it has been shown that intermolecular interactions of a dimer in the chosen configuration can lead to a large increase in the second hyperpolarizabilities. The molecular second hyperpolarizability values in the presence of a neighboring molecule represent a clear improvement over the isolated monomer values when compared to the experimental reference, although the agreement is not expected to be perfect due to the simplicity of the structural model. The remaining deviations, i.e., overestimation for furan and underestimation for tellurophene, possibly may be attributed to the details of the microscopic structure of the real liquid at a finite temperature, which we did not take into account in the present calculations. Moreover, in addition to the plane distance, other degrees of freedom such as the "slip" distance sketched in Figure 3 may have influence on the result.

It has been mentioned above that the calculated second hyperpolarizabilities can be qualitatively rationalized with the help of the excitation energy spectrum. Also here, the large increase of the molecular second hyperpolarizability is paralleled by a decrease in the lowest electronic excitations of the dimer with respect to the monomer. A selection of the lowest excitations for the monomer and the dimer of tellurophene are collected in Table 12 for the GRAC potential.

It can be seen that even the lowest excitations decrease substantially in energy. This observation can qualitatively be rationalized by MO-theoretical arguments, as illustrated schematically in Figure 4. Given the large HOMO−LUMO gap in the title molecules (about 4 eV), it can be assumed that the HOMO (in general, all the occupied levels) of one monomer primarily undergoes interaction with the HOMO of the other monomer, because the LUMO energy is too high to allow for significant mixing. This results in Pauli repulsion due to a 4-electron-2-orbital interaction, and the energy of the HOMO in the dimer is effectively pushed up relative to the HOMOs of the monomers. A similar interaction pattern can be derived for the LUMO-LUMO interaction, although the observed splittings are smaller. As a result, the HOMO−LUMO gap of the dimer is effectively reduced as compared to the individual monomers, thus resulting in a reduction of the lowest excitation energies.

In summary, we conclude that the presence of the surrounding molecules in the liquid phase may provide an explanation for the difference in second hyperpolarizability in the calculations

TABLE 12: Lowest Excitation Energies for the Tellurophene Monomer and Dimer; GRAC (eV)

monomer $\pi \rightarrow \pi^*$				dimer $(\pi\pi) \rightarrow (\pi\pi)^*$			
excit	eV	orbitals	weight %	excit	eV	orbitals	weight %
$1A_1$	4.50	$7b_1 \rightarrow 8b_1$	92	$1A_g$	3.79	$26a_g \rightarrow 27a_g$	66
						$26b_u \rightarrow 27b_u$	34
				$1B_u$	3.82	$26a_g \rightarrow 27b_u$	55
						$26b_u \rightarrow 27a_g$	45
				$4A_g$	4.49	$26b_u \rightarrow 27b_u$	62
						$26a_g \rightarrow 27a_g$	30
				$4B_u$	4.52	$26b_u \rightarrow 27a_g$	51
						$26a_g \rightarrow 27b_u$	40
$1B_2$	5.04	$3a_2 \rightarrow 8b_1$	90	$3B_g$	4.07	$14b_g \rightarrow 27a_g$	60
						$14a_u \rightarrow 27b_u$	40
				$3A_u$	4.08	$14b_g \rightarrow 27b_u$	59
						$14a_u \rightarrow 27a_g$	41
				$4B_g$	5.04	$14a_u \rightarrow 27b_u$	55
						$14b_g \rightarrow 27a_g$	35
				$4A_u$	5.06	$14a_u \rightarrow 27a_g$	53
						$14b_g \rightarrow 27b_u$	36

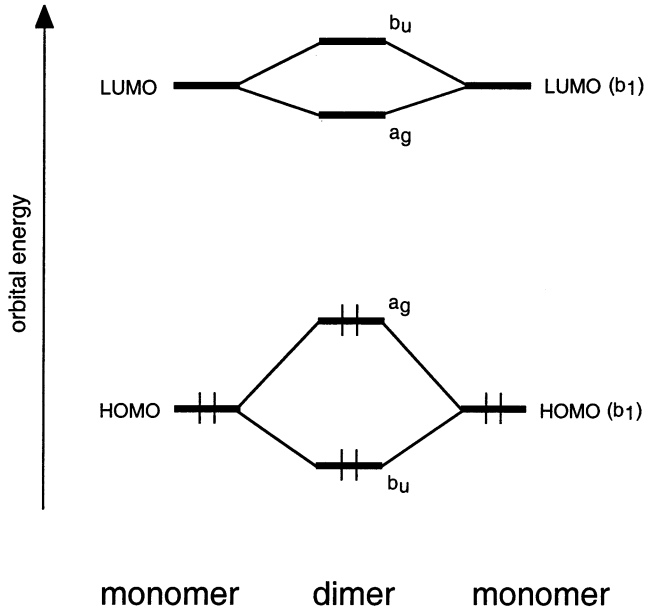

Figure 4. Schematic orbital interaction diagram for the dimer molecules.

on gas-phase monomers and in the experiment observed before. Hence, the large discrepancy found for tellurophene is probably not due to approximations made in the theoretical models used in the calculations.

4. Conclusions

In the present study, we have discussed the performance of current TDDFT methods for the accurate prediction of response properties for furan and its heavier homologues thiophene, selenophene, and tellurophene in comparison with recent ab initio and experimental data. In particular, we have investigated the electronic excitation spectra and the molecular second hyperpolarizabilities of the title compounds, and we have addressed several possible reasons for the large discrepancies found recently between experimental data and ab initio calculations.

The results show that TDDFT in combination with current exchange-correlation potentials, some of which have especially been designed for the calculation of response properties, can successfully be used to calculate the electronic excitation spectrum and second hyperpolarizabilities of the furan homologues. The TDDFT excitation energies to the lowest valence

states show rather little variance with the xc-potential employed. Greater differences show up for Rydberg excitations, where correct asymptotic behavior of the potentials is a prerequisite. Reasonable overall agreement between our TDDFT and ab initio results is obtained, especially for GRAC, although a final judgment is difficult due to significant scattering of the latter methods for furan and thiophene.

Second hyperpolarizabilities of the title molecules have been measured recently, but difficulties have been encountered in reproducing the experimental values by theory in earlier studies, especially for the heavier homologues, and several theoretical shortcomings such as basis sets, frequency dispersion, and relativistic effects have been suggested as possible explanations for the deviations. In the present study, we have investigated these suggestions by TDDFT calculations on the static and frequency-dependent second hyperpolarizabilties. Static values as currently available from sophisticated ab initio methods such as CCSD(T) are well reproduced by DFT provided suitable basis sets including an appropriate number and form of diffuse functions are used. LDA and the GGA BP86 perform surprisingly well, whereas the asymptotically corrected potentials LB94 and SAOP tend to underestimate the property. GRAC seems to be the most reliable and accurate choice within the five potentials applied here. More specifically, the values approach the CCSD(T) results closely and, moreover, are fairly stable with respect to basis set extension. A balanced description of valence and (at least) the lowest Rydberg excited states parallels good performance for hyperpolarizabilties, which is the case for GRAC, but not for SAOP and LB94. The traditional potentials LDA and BP86 seem to benefit from error cancellation.

The frequency dispersion contribution to the nonlinear response as estimated on the basis of our TDDFT results amounts to 21−36% and is similar to that previously calculated within TDHF theory and approximate extrapolation schemes. Scalar relativistic effects, as incorporated by the ZORA approach increase the second hyperpolarizability only slightly.

The influence of neighboring molecules, as present in the condensed phase, has been modeled by extending the calculations of isolated molecules in the gas phase to dimers as a first step. Although only a single configuration has been considered and the dynamical structure of the full liquid has been neglected, a much improved agreement between theoretical and experimental molecular second hyperpolarizabilities has been found. On the basis of our current data, we thus consider the influence of bulk effects on the second hyperpolarizability a possible explanation for the observed discrepancy between gas-phase calculations on the isolated five-ring molecules and the experimental condensed-phase results.

Acknowledgment. W.H. is grateful for support from the European Commission in the form of a Marie-Curie fellowship (Human Potential Program, HPMFCT-2000-00678). We are also grateful to the National Computing Facilities foundation (NCF) of The Netherlands foundation for Scientific Research (NWO) for a grant of computer time.

References and Notes

(1) Günter, P., Ed. *Nonlinear Optical Effects and Materials*; Springer: Berlin, 2000.

(2) Prasad, P. N.; Williams, D. J. *Introduction to Nonlinear Optical Effects in Molecules and Polymers*; John Wiley & Sons: New York, 1991.

(3) Fringuelli, F.; Marino, G.; Taticchi, A.; Grandolini, G. *J. Chem. Soc., Perkin Trans.* **1973**, 332.

(4) Kamada, K.; Ueda, M.; Sakaguchi, T.; Ohta, K.; Fukumi, T. *J. Opt. Soc. Am. B* **1998**, *15*, 838.

(5) Kamada, K.; Sugino, T.; Ueda, M.; Tawa, K.; Shimizu, Y.; Ohta, K. *Chem. Phys. Lett.* **1999**, *302*, 615.

(6) Kamada, K.; Ueda, M.; Nagao, H.; Tawa, K.; Sugino, T.; Shmizo, Y.; Ohta, K. *J. Phys. Chem. A* **2000**, *104*, 4723.

(7) Ohta, K.; Tanaka, T.; Kiyohara, K.; Tawa, K.; Kamada, K. *Synth. Met.* **2000**, *115*, 185.

(8) Millefiori, S.; Alparone, A. *Chem. Phys. Lett.* **2000**, *332*, 175.

(9) Millefiori, S.; Alparone, A. *Phys. Chem. Chem. Phys.* **2000**, *2*, 2495.

(10) Casida, M. E. In *Recent Advances in Density Functional Methods*; Chong, D. P., Ed.; World Scientific: Singapore, 1995; Vol. 1, pp 155.

(11) Gross, E. K. U.; Kohn, W. *Adv. Quantum Chem.* **1990**, *21*, 255.

(12) van Gisbergen, S. J. A.; Snijders, J. G.; Baerends, E. J. *J. Chem. Phys.* **1998**, *109*, 10644.

(13) van Gisbergen, S. J. A.; Snijders, J. G.; Baerends, E. J. *Comput. Phys. Commun.* **1999**, *118*, 119.

(14) Karna, S. P.; Dupuis, M. *J. Comput. Chem.* **1991**, *12*, 487.

(15) Bauernschmitt, R.; Ahlrichs, R. *Chem. Phys. Lett.* **1996**, *256*, 454.

(16) Bauernschmitt, R.; Häser, M.; Treutler, O.; Ahlrichs, R. *Chem. Phys. Lett.* **1997**, *264*, 573.

(17) Ceperly, D. M.; Alder, B. J. *Phys. Rev. Lett.* **1980**, *45*, 566.

(18) Vosko, S. H.; Wilk, L.; Nusair, M. *Can. J. Phys.* **1980**, *58*, 1200.

(19) Becke, A. D. *Phys. Rev. A* **1988**, *38*, 3098.

(20) Perdew, J. P. *Phys. Rev. B* **1986**, *33*, 8822; (erratum) *Phys. Rev. B* **1986**, *34*, 7406.

(21) van Leeuwen, R.; Baerends, E. J. *Phys. Rev. A* **1994**, *49*, 2421.

(22) Gritsenko, O. V.; Schipper, P. R. T.; Baerends, E. J. *Chem. Phys. Lett.* **1999**, *302*, 199.

(23) Grüning, M.; Gritsenko, O. V.; van Gisbergen, S. J. A.; Baerends, E. J. *J. Chem. Phys.* **2001**, *114*, 652.

(24) Derrick, P. J.; Asbrink, L.; Edqvist, O.; Jonsson, B.-Ö.; Lindholm, E. *Int. J. Mass Spectrom. Ion Phys.* **1971**, *6*, 161.

(25) Derrick, P. J.; Asbrink, L.; Edqvist, O.; Jonsson, B.-Ö.; Lindholm, E. *Int. J. Mass Spectrom. Ion Phys.* **1971**, *6*, 177.

(26) Distefano, G.; Pignataro, S.; Innorta, G.; Fringuelli, F.; Marino, G.; Taticchi, A. *Chem. Phys. Lett.* **1973**, *22*, 132.

(27) Fringuelli, F.; Marino, G.; Taticchi, A.; Distefano, G.; Colonna, F. P.; Pignataro, S. *J. Chem. Soc., Perkin Trans. 2* **1976**, 276.

(28) Cohen, H. D.; Roothaan, C. C. J. *J. Chem. Phys.* **1965**, *43*, S34.

(29) Bishop, D. M.; Kee, D. W. D. *J. Chem. Phys.* **1996**, *104*, 9876.

(30) Shelton, D. P. *J. Chem. Phys.* **1986**, *84*, 404.

(31) van Lenthe, E.; Baerends, E. J.; Snijders, J. G. *J. Chem. Phys.* **1993**, *99*, 4597.

(32) Bardo, R. D.; Ruedenberg, K. *J. Chem. Phys.* **1973**, *59*, 5956.

(33) Chong, D. P. Unpublished.

(34) Kaufmann, K.; Baumeister, W.; Jungen, M. *J. Phys. B*: *At. Mol. Opt. Phys.* **1989**, *22*, 2223.

(35) Guan, J. G.; Duffy, P.; Carter, J. T.; Chong, D. P.; Casida, K. C.; Casida, M. E.; Wrinn, M. *J. Chem. Phys.* **1993**, *98*, 4753.

(36) Zeiss, G. D.; Scott, W. R.; Suzuki, N.; Chong, D. P.; Langhoff, S. R. *Mol. Phys.* **1979**, *37*, 1543.

(37) te Velde, G.; Bickelhaupt, F. M.; Baerends, E. J.; Guerra, C. F.; van Gisbergen, S. J. A.; Snijders, J. G.; Ziegler, T. *J. Comput. Chem.* **2001**, *22*, 931.

(38) Modeli, A.; Guerra, M.; Jones, D.; Distefano, G.; Irgolic, K. J.; French, K.; Pappalardo, G. C. *Chem. Phys.* **1984**, *88*, 455.

(39) Norden, B.; Håkansson, R.; Pedersen, P. B.; Thulstrup, E. W. *Chem. Phys.* **1978**, *33*, 355.

(40) Flicker, W. M.; Mosher, O. A.; Kuppermann, A. *J. Chem. Phys.* **1976**, *64*, 1315.

(41) Cooper, C. D.; Williamson, A. D.; Miller, J. C.; Compton, R. N. *J. Chem. Phys.* **1980**, *73*, 1527.

(42) Roebber, J. L.; Gerrity, D. P.; Hemley, R.; Vaida, V. *Chem. Phys. Lett.* **1980**, *75*, 104.

(43) Palmer, M. H.; Walker, I. C.; Guest, M. F. *Chem. Phys.* **1999**, *241*, 275.

(44) Varsanyi, G.; Nyulazi, L.; Vezpremi, T.; Narisawa, T. *J. Chem. Soc., Perkin Trans. 2* **1982**, 761.

(45) Lonardo, G. D.; Galloni, G.; Trombetti, A.; Zauli, C. *J. Chem. Soc., Faraday Trans. 2* **1972**, 2009.

(46) Trombetti, A.; Zauli, C. *J. Chem. Soc. A* **1967**, 1106.

(47) Wan, J.; Meller, J.; Hada, M.; Ehara, M.; Nakatsuji, H. *J. Chem. Phys.* **2000**, *113*, 7853.

(48) Wan, J.; Hada, M.; Ehara, M.; Nakatsuji, H. *J. Chem. Phys.* **2001**, *114*, 842.

(49) Serrano-Andres, L.; Merchan, M.; Nebot-Gil, I.; Roos, B. O.; Fülscher, M. *J. Am. Chem. Soc.* **1993**, *115*, 6184.

(50) Serrano-Andres, L.; Merchan, M.; Fülscher, M.; Roos, B. O. *Chem. Phys. Lett.* **1993**, *211*, 125.

(51) Christiansen, O.; Jorgensen, P. *J. Am. Chem. Soc.* **1998**, *120*, 3423.

(52) Christiansen, O.; Halkier, A.; Koch, H.; Jorgensen, P. *J. Chem. Phys.* **1998**, *108*, 2801.

(53) Palmer, M. H.; Walker, I. C.; Ballard, C. C.; Guest, M. F. *Chem. Phys.* **1995**, *192*, 111.

(54) Trofimov, A. B.; Schirmer, J. *Chem. Phys.* **1997**, *224*, 175.
(55) Tozer, D. J.; Amos, R. D.; Handy, N. C.; Roos, B. O.; Serrano-Andres, L. *Mol. Phys.* **1999**, *97*, 859.
(56) Almbladh, C.-O.; von Barth, U. *Phys. Rev. B* **1985**, *31*, 3231.
(57) Perdew, J. P.; Parr, R. G.; Levy, M.; Balduz, J. L. *Phys. Rev. Lett.* **1982**, *49*, 1691.
(58) Chong, D. P. *Can. J. Chem.* **1995**, *73*, 79.
(59) van Gisbergen, S. J. A.; Snijders, J. G.; Baerends, E. J. *J. Chem. Phys.* **1998**, *109*, 10657.
(60) Orr, B. J.; Ward, J. F. *Mol. Phys.* **1971**, *20*, 513.
(61) Bredas, J. L.; Adant, C.; Tackx, P.; Persoons, A.; Pierce, B. M. *Chem. Rev.* **1994**, *94*, 243.
(62) Fringuelli, F.; Taticchi, A. *J. Chem. Soc., Perkin Trans. 1* **1972**, 199.
(63) Bondi, A. *J. Phys. Chem.* **1964**, *68*, 441.
(64) Nakano, H.; Tsuneda, T.; Hashimoto, T.; Hirao, K. *J Chem. Phys.* **1996**, *104*, 2312.